Available online at www.sciencedirect.com
SCIENCE DIRECT®
Journal of Catalysis 231 (2005) 331–343
JOURNAL OF CATALYSIS
www.elsevier.com/locate/jcat

Catalysis in membrane reformers: a high-performance catalytic system for hydrogen production from methane

P. Ferreira-Aparicio [a,*], M. Benito [a], K. Kouachi [b], S. Menad [b]

[a] *Instituto de Catálisis y Petroleoquímica, C/Marie Curie, s/n 28049 Madrid, Spain*
[b] *Département de Chimie, Faculté des Sciences, Université Mouloud Mammeri, Tizi-Ouzou, Algeria*

Received 11 November 2003; revised 8 August 2004; accepted 2 December 2004
Available online 17 March 2005

Abstract

A palladium membrane reactor has been designed and sized to be applied to the dry reforming of methane for pure hydrogen production at a small scale. Three different parameters affecting the reactor operation have been adjusted to tune the reformer and optimise its performance: the extraction conditions, the CO_2/CH_4 ratio in the reactant mixture composition, and the reactants feed flow rate. By forcing H_2 extraction and adjusting the rates of hydrogen production in the reactor and hydrogen permeation through the Pd membrane, it has been possible to obtain very high CH_4 conversion for mixtures with CO_2/CH_4 ratios above unity. Reactant mixtures with CO_2/CH_4 ratios close to 2 offered the best results: high H_2 recovery yields (above 95%) and lower carbon deposition in the catalysts under the severe conditions imposed by the membrane reactor operation. Hydrogen extraction from the reaction side has been shown to enhance the carbon deposition rate on nickel-based reforming catalysts, in which the formation of low-reactivity carbon in the form of fibres has been observed. The dispersion of nickel on high oxygen mobility supports, such as Ce–Zr mixed oxides ($Ce_{0.5}Zr_{0.5}O_2$), which are chemically stable under reaction conditions, results in highly efficient catalysts capable of keeping their surface free of inactive carbon deposits. This kind of oxide provides an extra source of oxygen that equilibrates the net rates of carbon deposition and removal on the nickel surface, thus avoiding the accumulation of carbon in the catalyst.

Keywords: Palladium membrane reformer; Hydrogen production; Dry methane reforming; Carbon nanofibres; Ni/Al_2O_3; $Ni/Ce_{0.5}Zr_{0.5}O_2$; Ni/ZrO_2; Ni/ZrO_2–CeO_2

1. Introduction

Although hydrogen production has been a matter of great importance in recent decades, a renewed interest in its production processes has emerged recently, driven by the spectacular advances in fuel cell technology. Up to now only a small fraction of the hydrogen produced is currently used for energy purposes, but the implementation of fuel cell systems and the growing demand for zero-emission fuels in the near future will increase the hydrogen share of the energy market. Its production from abundant sources in an economical way and with reduced purification costs would make possible the commercialisation of fuel cell-powered systems.

Large-scale hydrogen production from natural gas by steam reforming or autothermal reforming is a well-known process that uses purification methods such as pressure swing adsorption or cryogenics. However, H_2 production at a smaller scale from fossil fuels requires further investigation to meet the requirements of purity, economics, and versatility for its use in fuel processor systems to be coupled to fuel cells [1]. The utilisation of membrane reactors for this purpose is one of the most interesting options to consider, given its advantages related to heat and energy management, and the integration of two different processes (reaction and separation) in a single step.

* Corresponding author. Fax: +34 91 585 47 60.
E-mail address: pferreira@icp.csic.es (P. Ferreira-Aparicio).

0021-9517/$ – see front matter
doi:10.1016/j.jcat.2004.12.025

Several types of membranes have been tested in methane-reforming reactions for hydrogen separation: ceramic membranes [2,3], porous Vycor glass membranes [4–6], and palladium-based films [7–10]. However, the application of these modules to methane-reforming processes poses additional difficulties compared with other dehydrogenation reactions.

The small differences in the kinetic diameters of reactants and products usually reduce the permselectivity in porous membranes to the values corresponding to a Knudsen-type diffusion mechanism of the different species [3]. Because of this, dense membranes, whose operation is based on a H_2 solution-diffusion mechanism on a permselective film, are usually the preferred choice. Although metals such as Nb, Ta, V, and Zr and their alloys, particularly V–Ni, have greater hydrogen permeability than Pd, they have greater surface resistance to hydrogen transport due to their easier oxidation. On the other hand, the high operation temperature required for these reforming reactions limits the structural stability of H_2 permselective films and the utilisation of materials for membrane synthesis, fitting, sealing, enamelling, etc. As a result, the reactor performance becomes limited and controlled by numerous parameters, such as the thermal stability of its components, their mechanical resistance, their geometry, the membrane permeability and selectivity, not to mention the catalyst stability under the more severe reaction conditions imposed by the removal of hydrogen from the reaction medium, which finally remains one of the most important issues in the design of an efficient fuel processor. Up to now, most of the efforts in this field have been focused on the membrane itself and/or the reactor characteristics, but little attention has been devoted to the catalyst behaviour under the membrane reactor operation conditions. This latter question remains one of the most important challenges to be broached for these systems. Usually, noble metals have been used in membrane reactors to overcome problems related to carbon deposition [11,12]. However, their high price drives the development of alternative catalysts for this process. Some simulation studies concerning the catalytic performance of membrane reactors in the steam reforming of methane have been published in recent years [13–15]. In particular, Hou et al. noted in their study the increased tendency towards catalyst poisoning by carbon deposition and the stronger effect of contaminants such as H_2S when hydrogen is removed from the reaction zone [15], especially at temperatures below 873 K and pressures below 6 bar. In the case of the dry reforming of methane, the tendency towards carbon formation on the catalyst is even higher.

This communication reports a detailed study of different parameters influencing the operation of a membrane reformer for methane, with carbon dioxide as oxidant; the extraction conditions, the feed flow rate, and the reactant mixture composition have been adjusted to optimise the system performance. Several nickel-based catalysts dispersed on different supports have been prepared and tested in the membrane reactor. This study analyses the catalytic stability and resistance to carbon deposition of the different samples, revealing that the catalytic behaviour of the nickel-based systems strongly depends on the support characteristics. The design of high oxygen mobility supports that are chemically stable under the severe reaction conditions imposed by the reactor is the key for obtaining an active and stable catalytic system capable of long-term operation in a membrane reformer.

2. Experimental

2.1. Pd membrane preparation and characterisation

Palladium membranes were prepared by electroless plating deposition on the external surface of a porous 316L stainless-steel (PSS) support from Mott Corp. According to the manufacturer's specifications, the grade of the PSS was 0.5 μm, with an average pore diameter of 3 μm and a porosity of 17%. The permeable zone of the membrane module was designed to have a volume of approximately 2 cm^3 (o.d. 9.5 mm, wall thickness 1.6 mm, length 60 mm). The porous part was welded at both extremes to two 15-cm-long pieces of nonporous 316L stainless steel.

The membrane synthesis involved cleaning of the support, followed by successive sensitising, activation, and plating cycles according to the procedure described by Mardilovich et al. [16]. The activation procedure consisted of successive immersions in an acidic $SnCl_2$ bath (sensitising) and in deionised water, followed by an acidic $PdCl_2$ bath at room temperature. Then the membranes were rinsed with 0.01 M HCl and with deionised water to prevent hydrolysis of the Pd^{2+} ions. After several sensitizing/activation cycles, palladium was deposited at 333 K by an autocatalytic reduction reaction with the use of a plating bath consisting of a basic solution of $Pd(NH_3)_4Cl_2$, NaEDTA, and N_2H_4. Plating was followed by drying at 393 K. After each plating cycle, the membranes were tested for He permeation at room temperature to check for the absence of pores in the palladium film. Membranes that were not dense were submitted to another activation and plating cycle. Dense membranes were used for reaction experiments. This procedure made it possible to synthesise dense palladium membranes with a minimum thickness and maximise the H_2 permeation rate. The thickness of each Pd layer obtained in this way was estimated from the weight increase of the module.

The membrane tube was fixed to a stainless-steel shell with an inlet and an outlet to feed a sweep gas stream. The use of independent Swagelok fittings with graphite ferrules to integrate the membrane in the reactor and to connect it to the experimental setup provided an easily handled gas-tight seal, which avoided leakage problems between the retentate and the permeate sides.

The permeation properties of the synthesised membranes were evaluated for He and H_2 at several temperatures be-

tween 623 and 823 K. Selectivity for hydrogen separation was estimated from single gas permeation experiments.

2.2. Catalyst preparation and characterisation

A series of supported nickel catalysts was prepared for the membrane reactor operation. Four different supports were used: Al_2O_3 (Puralox Condea), ZrO_2 (Mel Chemicals), ZrO_2–CeO_2 (Mel Chemicals), and a Ce–Zr mixed oxide with a Zr:Ce atomic ratio of 1.

The ZrO_2 support contained 3.5 wt% SiO_2 to stabilise the zirconia tetragonal phase. It was obtained by calcination of its hydroxide at 973 K. The ZrO_2–CeO_2 support, according to the manufacturer's specifications, had a CeO_2 content of 17.5 wt%. Finally, a mixed oxide with a Zr/Ce ratio of 1:1 was prepared by the water-to-oil microemulsion method according to the procedure described in [17].

We tested the oxygen exchange ability of the prepared supports in a volumetric glass system by cycling at 923 K a known amount of $^{18}O_2$ through the sample, while analyzing with a quadrupole mass spectrometer (Balzers QMS 421) the evolution with time of the gas-phase composition.

Nickel catalysts with 5 wt% metal loading were prepared on the above-mentioned supports by the incipient wetness impregnation technique with aqueous solutions of $Ni(NO_3)_2$ (Alfa). After the samples were dried overnight at room temperature, the catalysts were calcined in air at 823 K. Catalysts were pressed and sieved to particle sizes ranging from 0.42 to 0.59 mm.

2.3. Membrane reactor operation

For operation, the maximum temperature in the external furnace was fixed at 823 K because intermetallic diffusion between palladium and iron is known to cause the hydrogen permeation flux in the membrane to decay at higher temperatures [16]. The system was not exposed to H_2 at temperatures below 573 K to avoid hydrogen embrittlement in the palladium layer. Special care was taken during the heating and cooling processes, in which the temperature was varied at low rates (1 K min^{-1}) under an inert gas flow.

Some preliminary catalytic tests were carried out in a conventional reactor to determine the amount of catalyst to be loaded in the membrane according to its specific activity for the reaction. For reaction tests, the catalyst was loaded inside the membrane tube, between two quartz wool plugs, all along the permeation zone, and the experimental conditions were changed to explore the system performance. It should be noted that the reaction temperature was 20–40 °C lower than the external temperature, depending on the operation conditions. The temperature in the middle of the catalytic bed was determined with a second thermocouple inserted along the membrane in the reaction side.

We carried out the methane-reforming reaction by feeding mixtures of CH_4 and CO_2 in different proportions without any diluents. The influence of three parameters on the reaction was analysed: the reactant mixture composition, the sweep gas flow rate, and the reactant feed rate.

2.4. Catalyst resistance to carbon deposition

A series of experiments was carried out for the different catalysts in the membrane reactor under the same conditions (temperature, extraction flow rate, reactant feed flow rate, reactant mixture composition) to determine their resistance to carbon deposition. After 24 h in operation, spent catalysts were examined by scanning electron microscopy, and their carbon deposits were determined by gravimetric analysis after calcination at 1173 K. The reactivity with hydrogen of the carbon deposits formed on the several catalysts was also studied by temperature-programmed hydrogenation. Finally, the residual coke remaining on the catalysts after hydrogenation at 1073 K was also gravimetrically determined.

To clarify the effect of hydrogen removal during reaction, these experiments were also carried out for the several catalysts in a conventional reactor. They were tested under comparable conditions by replacing the membrane module with a nonporous stainless steel tube of identical dimensions to avoid differences due to the thermal conductivity of the reactor material and its geometry, the catalyst disposition in the reactor, and temperature effects.

3. Results and discussion

3.1. Preliminary catalytic study

The Ni/Al_2O_3 catalyst was initially used for the study of the different factors affecting the membrane reactor behaviour, as it is known to be one of the most efficient catalytic systems for carrying out hydrocarbon reforming reactions and, in particular, the dry reforming of methane [18]. A preliminary catalytic study was carried out on this catalyst under differential conditions in a conventional reactor to determine its specific activity and catalytic properties for the CH_4/CO_2 reaction. Table 1 summarises the catalytic activity of this sample for CH_4 conversion at different CO_2/CH_4 ratios in the feed mixture composition. Other parameters, such as the CO/H_2 ratio after reaction and the selectivity for H_2, are also included.

Table 1
Catalytic properties of the Ni/Al_2O_3 catalyst for the dry reforming of methane

CO_2/CH_4 feeding	A_{CH_4} (μmol g^{-1} s^{-1})	X_{CH_4} (%)	CO/H_2	S_{H_2} (%)
1.0	42.6	11.3	1.5	80
1.9	42.7	11.2	2.0	67
2.8	33.1	8.7	2.7	54
3.8	28.3	7.5	3.3	46

Reaction conditions: catalytic bed temperature, 783 K; pressure, 1 atm; CH_4 feed flow rate, 5.95×10^{-6} mol/s.

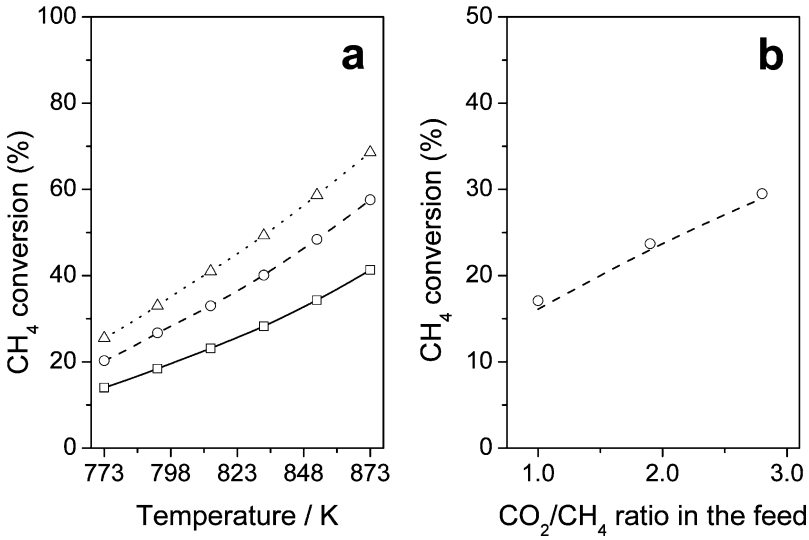

Fig. 1. (a) Theoretical values for equilibrium methane conversion in the dry methane reforming as a function of temperature for different CO_2/CH_4 ratios in the feeding: $CO_2/CH_4 = 1$ (–□–), $CO_2/CH_4 = 2$ (- -○- -) and $CO_2/CH_4 = 3$ (··△··). (b) Methane conversion as a function of the CO_2/CH_4 ratio at 783 K. Circles, experimentally determined data. Dashed line, theoretical values.

It can clearly be seen that as long as the CO_2/CH_4 ratio in the reactant mixture increases, CH_4 conversion and H_2 selectivity decay, and the CO/H_2 ratio increases. The CO_2 excess in the reactant mixture with respect to the dry reforming reaction stoichiometry ($CH_4 + CO_2 \Longleftrightarrow 2H_2 + 2CO$) favours the occurrence of the reverse water gas shift (RWGS) reaction ($CO_2 + H_2 \Longleftrightarrow CO + H_2O$). This secondary process consuming CO_2 and the produced H_2 leads to a large increase in the CO/H_2 ratio in the outlet stream while producing H_2O in the reaction medium. The decrease observed in the specific activity for CH_4 decomposition with an increasing CO_2/CH_4 ratio in the feed is not due to deactivation of catalytic sites but to the competition of the parallel RWGS reaction for the nickel adsorption centres. Although the utilisation of a CO_2 excess in the reaction mixture can be unfavourable from the standpoint of H_2 production in terms of selectivity, thermodynamics suggests the operation of the dry methane reforming with CO_2/CH_4 ratios far above unity to avoid regions with a thermodynamic potential for carbon formation [19]. This is an important consideration to take into account when a membrane reactor is used to extract the hydrogen produced from the reaction medium.

Under equilibrium conditions, a higher CO_2/CH_4 ratio in the feed also causes CH_4 conversion to increase, according to Le Chatelier's principle. Fig. 1a shows the estimated CH_4 conversion under equilibrium conditions as a function of the reaction temperature for different CO_2/CH_4 ratios in the feed. These conversion data have been calculated from the equilibrium constants, which were determined from the Gibbs free energy values of reactants and products at different temperatures according to the reaction stoichiometry [20]. The experimentally determined values in a conventional reactor under equilibrium conditions (Fig. 1b) have shown a good concordance with those theoretically calculated at the temperature measured during reaction in the middle of the catalytic bed. It must be considered that although the increase in the CO_2/CH_4 ratio leads to a higher CH_4 conversion under the conditions dictated by thermodynamics (Fig. 1), with respect to the specific activity of the catalyst measured under differential conditions (Table 1), the increase in the CO_2/CH_4 value causes the specific activity of the catalyst to decrease, and a higher amount of catalyst is required to achieve equilibrium.

3.2. Membrane reactor tests: adjustment of extraction conditions, reactant mixture composition, and reactant feed rate

On the basis of the previous results, several tests were carried out with the membrane reactor to explore its behaviour. We estimated the mass of catalyst to be loaded into the reactor by considering the specific catalytic activity of the reforming catalyst (Ni/Al_2O_3) and the permeability range of the membranes. The thickness of the prepared palladium films ranged from 12 to 35 μm, with permeances for H_2 between 6.4×10^{-5} and 28.6×10^{-5} $mol\,m^{-2}\,s^{-1}\,Pa^{-0.5}$ measured at a temperature of 783 K. Values for hydrogen permeance were determined from the measurement of the hydrogen flux across the membranes at 783 K as a function of the difference in pressure between the two sides of the membranes. Hydrogen flux was observed to be directly proportional to ($P^{0.5}$–$P_0^{0.5}$) values corresponding to the transmembrane pressure difference, in agreement with Sievert's law for hydrogen solubility in palladium. Depending on the Pd film thickness of the membrane module used for each experiment, the maximum rate for hydrogen permeation at 783 K for a H_2 transmembrane pressure difference of 40 kPa oscillated between 2×10^{-5} and 9×10^{-5} $mol\,s^{-1}$. For this permeance, approximately 1 g of sample was loaded along the porous zone and reduced under pure hydrogen at the re-

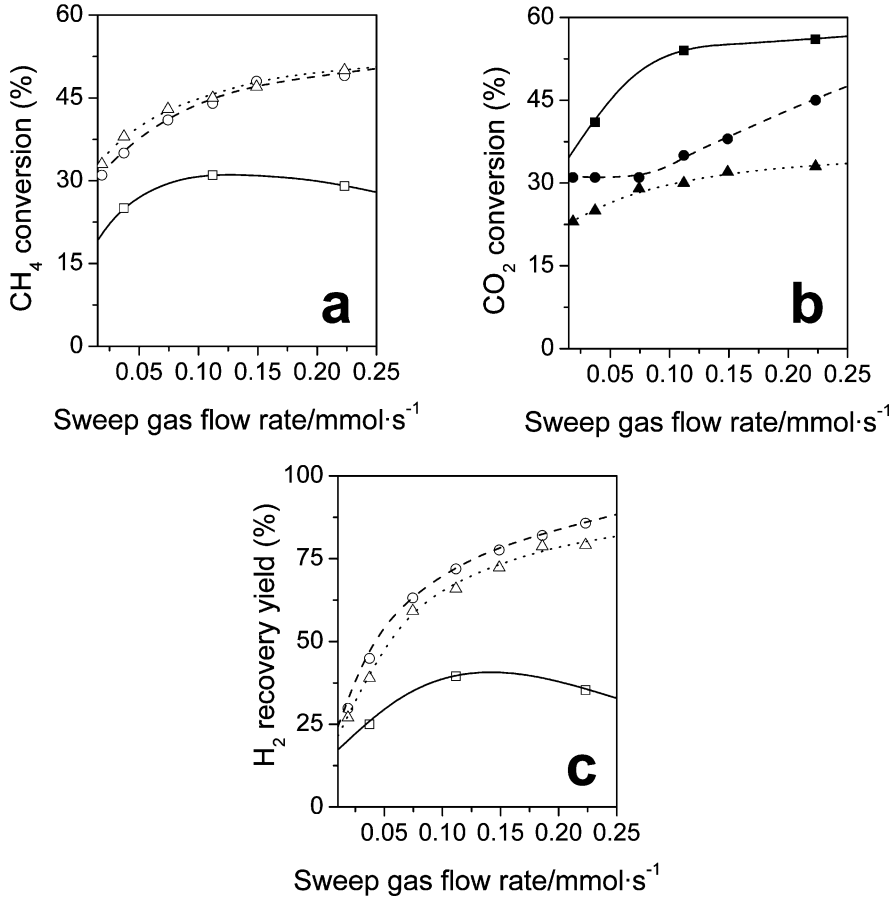

Fig. 2. Effect of the sweep gas flow rate on the reactor performance for several CO_2/CH_4 ratios: (a) methane conversion, (b) carbon dioxide conversion, and (c) hydrogen recovery yield. $CO_2/CH_4 = 1$ (–□–), $CO_2/CH_4 = 2$ (- -○- -), and $CO_2/CH_4 = 3$ (··△··).

action temperature. At the previously indicated temperature and with the mass of catalyst loaded, the system was able to convert CH_4 at a rate of at least 3×10^{-5} mol s^{-1} for CO_2/CH_4 ratios lower than 3 and produce H_2 at a rate of 6×10^{-5} mol s^{-1} g^{-1}. The amount of catalyst loaded was enough to ensure that the system would not operate limited by the catalytic activity of the catalyst, as the maximum conversion rate was similar or even higher than the permeation rate at a hydrogen transmembrane pressure of 40 kPa. Taking into consideration these estimates, the reactant mixture composition, the extraction conditions, and the reactant feed rate were adjusted to optimise the system performance.

First, two different parameters were changed: the reactant mixture composition and the extraction conditions. As the driving force for hydrogen permeation through the membrane is proportional to the H_2 partial pressure difference across the Pd film, it is possible to produce a permeance rate increase by reducing the total pressure at the shell side during the reaction or by using a sweep gas flow that causes the hydrogen partial pressure to come down at the shell side. In this case a He stream was used as a sweep gas, showing an important effect on the reactor behaviour. As a general rule, when the sweep gas flow rate increases, the membrane operation improves progressively because of a faster H_2 extraction from the reaction medium. However, the reactor performance greatly depends on the reactant mixture.

Fig. 2 compiles the CH_4 and CO_2 conversion levels obtained in the membrane reactor and the H_2 recovery yield as a function of the sweep gas flow rate for three different CO_2/CH_4 ratios ranging from 1 to 3. The recovery yield is defined as the percentage of hydrogen obtained at the shell side relative to the hydrogen content in the converted CH_4. As shown in Fig. 2a, a reactant feeding with a CO_2/CH_4 ratio close to unity causes CH_4 conversion to rise when moderated extraction conditions are applied. For very high sweeping flow rates, CH_4 conversion decays. At the same time, CO_2 conversion continues rising moderately because of its reaction with carbon species formed from methane and the remaining H_2 (Fig. 2b). These conditions are not suitable to maintain or increase the CH_4 conversion level in the reactor, as the CO concentration is too high in the reaction side. In terms of hydrogen recovery, it can be seen that very high sweeping gas flow rates cause the H_2 yield to decrease slightly, in concordance with the lower CH_4 conversion.

For mixtures with higher CO_2/CH_4 ratios, the use of high sweep gas flow rates led to a continuous conversion increase associated with an enhanced H_2 recovery. These results in-

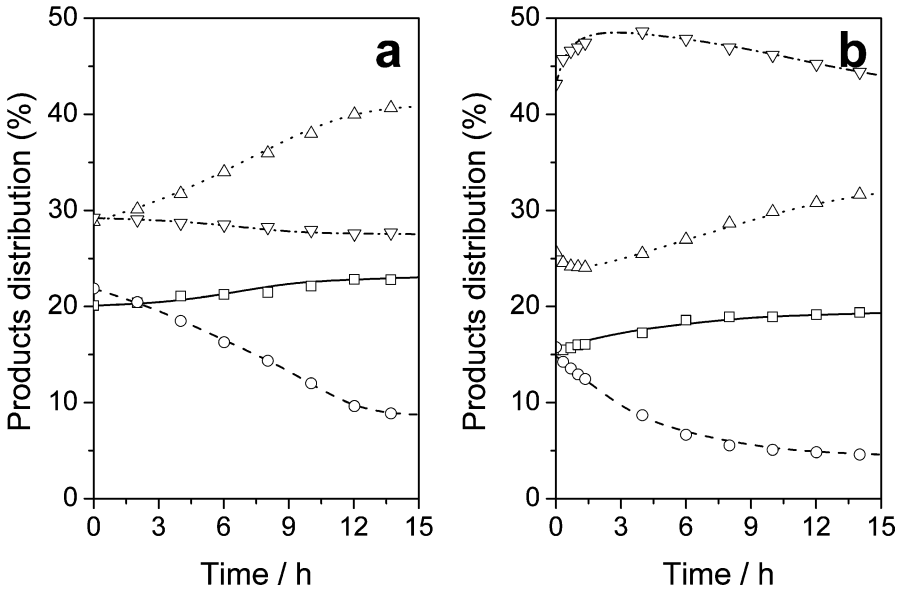

Fig. 3. Composition variation in the reaction side of the membrane reactor along with time: H_2 (–□–), CH_4 (- -○- -), CO (··△··), and CO_2 (··▽··). (a) $CO_2/CH_4 = 1$; (b) $CO_2/CH_4 = 2$. Sweep gas flow rate, 3.72×10^{-5} mol s^{-1}.

dicate that a certain CO_2 excess in the feed with respect to the stoichiometric ratio establishes more favourable conditions for reactor operation. However, the CO_2 surplus in the feeding must be limited to a certain level to reduce as much as possible H_2O formation through the RWGS, given that the hydrogen recovery yield becomes reduced for too high CO_2/CH_4 ratios.

The observed behaviour is the result of a variety of factors involved in the whole reactor performance: the hydrogen concentration in the reaction side, which depends on the reactant mixture composition, the CH_4 conversion level and the sweeping conditions, the presence of secondary reactions consuming hydrogen from the reaction medium, and the equilibration of all of these processes, which are interrelated. The system equilibration is a complex process, as can be inferred from the time needed to reach a stationary state in the reaction side composition when low sweep gas flow rates are used (Fig. 3). For an equimolecular CH_4/CO_2 mixture (Fig. 3a) or a feed with a CO_2/CH_4 ratio of 2 (Fig. 3b), H_2 concentration inside the membrane remains almost constant between 16 and 22 vol% when a sweep gas stream of 0.037 mmol s^{-1} flows at the shell side. However, CH_4 proportion becomes greatly reduced with time because of a higher conversion level driven by H_2 removal through the membrane. This CH_4 conversion enhancement causes CO concentration to increase. On the other hand, CO_2 conversion variation is more evident when an excess of CO_2 (Fig. 3b) is used, although a similar tendency can be envisaged in both cases. Initially the CO_2 concentration increases because of the RWGS reaction avoidance produced by H_2 removal, but its proportion in the reaction side is gradually reduced as result of its consumption associated with CH_4 conversion. The larger increment in CH_4 conversion as compared with that of CO_2 also reveals the inhibition of the reaction between H_2 and CO_2. With higher sweeping gas flow rates, the equilibrium situation is reached faster.

It is possible to further reduce the H_2 content in the reaction side by forcing the hydrogen extraction conditions with the use of reaction mixtures containing excess CO_2. To maximise the H_2 recovery yield it is also necessary to adjust the hydrogen production and permeation rates. Therefore, the reactant mixture composition and the extraction conditions are fixed, the reactant feed flow rate would have to be regulated to tune the reactor and optimise its performance. Fig. 4a shows the effect of reducing the CH_4 feed flow rate on conversion. The CO_2/CH_4 ratio in the reactant mixture was maintained at 1.9, and a sweeping stream of 0.223 mmol s^{-1} was used. A large conversion increase was observed when the CH_4 flow rate was reduced below 3.5×10^{-5} mol s^{-1}. It should be noted that for the entire range tested (from 6×10^{-6} to 7.2×10^{-5} mol s^{-1} of CH_4) the reaction was not limited by the amount of loaded catalyst. The rate of hydrogen production varied between 8.0×10^{-6} mol s^{-1} (for the lowest feeding flow rate and the highest conversion) and 4.3×10^{-5} mol s^{-1} (for the highest feeding flow rate and lowest conversion). By varying the feeding rate, no significant modification is observed in the hydrogen permeation rate through the membrane. Assuming that under those conditions the used membrane is able to extract H_2 at a rate of 8.4×10^{-6} mol s^{-1}, the reduction of the hydrogen formation rate to the same level as the permeation allows conversion to increase to three times the equilibrium conversion level (23%) with a hydrogen recovery yield above 95%, as shown in Fig. 4b.

Several studies have analysed parameters that influence membrane reformer operation. They concur in noting the importance of variables such as the load-to-surface ratio (L/S) or the weight hourly space velocity (WHSV) [9,21–23]. In

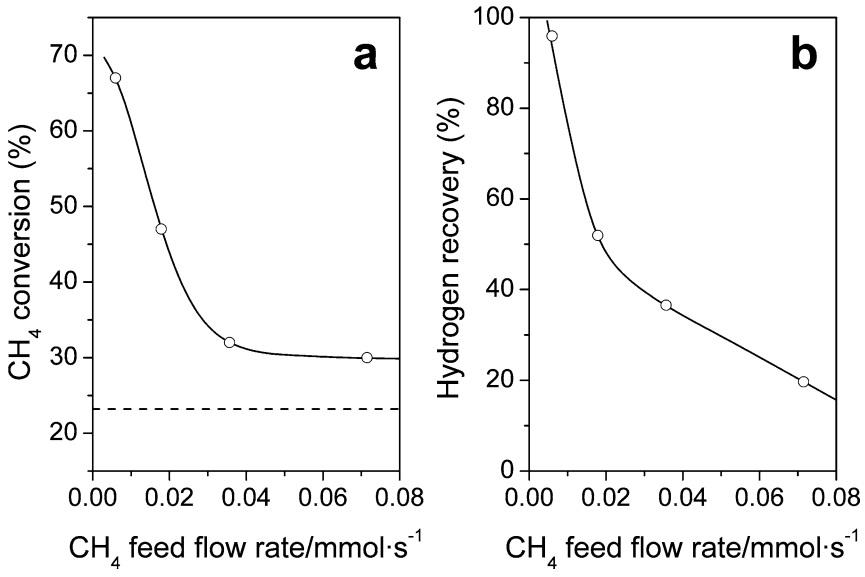

Fig. 4. Effect of the CH_4 feed flow rate on (a) the methane conversion and (b) the hydrogen recovery yield. Dotted line in (a): equilibrium conversion.

particular, Lin et al. have studied the steam methane reforming in a Pd membrane reactor by modelling its behaviour as a function of these two major working parameters: the WHSV of CH_4 and the L/S in the membrane [10]. In agreement with our results, they have found a large conversion enhancement by decreasing the CH_4 WHSV and the L/S ratio. However, their calculation indicates that conversion does not reach the maximum value (100%), even for a large enough membrane area (low L/S) or for low WHSV due to H_2 removal limitations, which are imposed by the experimental extraction conditions and the membrane. In the case of the application of a pressure difference between the reaction and permeation side, further conversion improvement can be achieved with a sweep gas stream and vice versa.

3.3. Nickel-based reforming catalysts: resistance to carbon deposition

The previous results will now allow us to study one of the most important components of the reactor: the reforming catalyst. Four different nickel-based catalysts were tested: Ni/Al_2O_3, Ni/ZrO_2, Ni/ZrO_2–CeO_2, and $Ni/Ce_{0.5}Zr_{0.5}O_2$. Their catalytic behaviour with respect to carbon deposition has been studied and analysed after operation in the membrane reactor under the previously established optimum reaction conditions. For these experiments, the membrane reactor was fed with a mixture of CO_2/CH_4 at a ratio of 1.9 and at a total flow rate of 5.97×10^{-6} mol s^{-1} and atmospheric pressure. H_2 was extracted with a sweep gas flow rate of 0.223 mmol s^{-1}. It is worth noting the high CO concentration in the effluent coming from the reaction side of the membrane reactor under these conditions, even when a mixture with a CO_2/CH_4 ratio close to 2 is used. During operation, the CO concentration in the outlet gas composition exceeds 35 vol%, although CO_2 is maintained at a high level (46 vol%) to reduce CO disproportionation in the reaction side. (In a conventional reactor CO and CO_2 concentrations for identical conditions of temperature and feed are 20 and 44 vol%, respectively.)

Table 2
Weight increase due to carbon deposition for the different nickel catalysts after 24 h operation in the membrane (MR) and traditional (TR) reactors

Catalyst	Ni (wt%)	S_{BET} ($m^2\,g^{-1}$)	MR		TR	
			ΔW (mg/g_{cat})	C_{hydrog} (%)	ΔW (mg/g_{cat})	C_{hydrog} (%)
Ni/Al_2O_3	4.9	178	545	29	18	100
Ni/ZrO_2	4.4	110	464	21	81	45
Ni/ZrO_2–CeO_2	4.8	68	615	2	580	2
$Ni/Ce_{0.5}Zr_{0.5}O_2$	4.4	62	33	100	45	100

Ni (%), nickel loading in wt%.
S_{BET}, catalyst specific surface area.
ΔW, gravimetric determination of the deposited carbon in spent catalysts after its calcination in air at 1173 K.
C_{hydrog}, percentage of hydrogenatable carbon from the total amount deposited.

Table 2 compiles some of the catalyst characteristics and the carbon deposition on them after 24 h of operation in the membrane reactor and after 24 h of operation in a traditional reactor under identical conditions but without hydrogen extraction. It is clear from the results that, in the case of catalysts such as Ni/Al_2O_3 or Ni/ZrO_2, hydrogen extraction from the reaction medium favours faster carbon deposition on the catalyst surface. However, it should be noted that no deactivation was observed in the reactors, although a significant pressure drop appeared progressively in the cases where catalysts with very high coke deposition rates were used (Ni/ZrO_2–CeO_2). These results indicate that, despite the high coking rate on the catalysts, the nickel surface sites remain free for reactant activation. Moreover, it is important to consider that catalyst fractions located at different heights in a 5-cm-long fixed-bed reactor operate under different local reaction atmospheres, differences that become even more

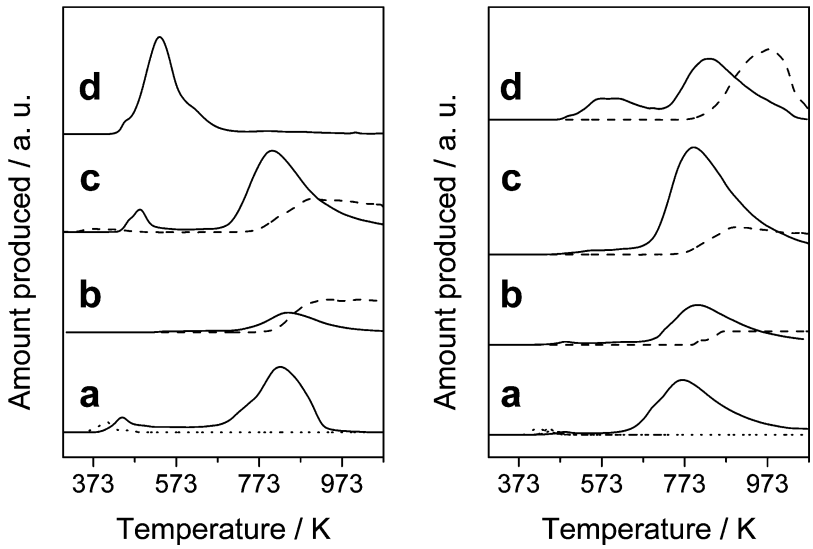

Fig. 5. Temperature programmed hydrogenation experiments for the supported nickel catalysts: (a) Ni/Al_2O_3, (b) Ni/ZrO_2, (c) Ni/ZrO_2–CeO_2, and (d) $Ni/Ce_{0.5}Zr_{0.5}O_2$. Left side, after 24 h operation in a traditional reactor. Right side, after 24 h operation in the palladium membrane reactor. Solid line, CH_4 production. Dashed line, CO production. Dotted lines, C_2–C_3 hydrocarbons.

pronounced in the case of a membrane removing H_2 from the reaction medium. Thus, under the conditions used, a higher carbon deposition at the end of the catalytic bed due to the occurrence of the CO disproportionation reaction ($2CO \Longleftrightarrow C + CO_2$) is expected.

A recent study regarding the use of fixed- and fluidised-bed reactors applied to dry methane reforming with Ni/SiO_2 catalysts reveals the superior performance of fluidised bed reactors over fixed-bed reactors. In these latter reactors it is confirmed that the used catalysts show a non-uniform coke distribution deposited mainly at the end of the bed via the Boudouard reaction [24]. The authors attribute catalyst deactivation to the formation of less reactive carbon species caused by a lower CO_2/CH_4 ratio in that zone. That study was carried out with a clean model biogas with a CO_2/CH_4 ratio of 1.0. In our case, the CO_2 excess in the reactant acts as a "moderator" of the Boudouard reaction. Froment has recently remarked the importance of modelling the behaviour of steam and CO_2 reformers to simulate the net rate of carbon formation on Ni catalysts [25]. This kind of study provides better insight into the role of the numerous variables influencing carbon deposition, which increases with the distance in the catalytic bed and a higher CH_4 partial pressure in the feed. Wurzel et al. have also stressed in their studies the performance improvement obtained when fluidised bed reactors are used for the CO_2 reforming of CH_4 [26]. They have attributed this better performance to lower deactivation rates in the catalyst caused by the solid mixing into the CO_2-rich distribution zone, where carbon deposits are removed by the reverse Boudouard reaction.

As can be inferred from the results in Table 2, apart from the operation conditions imposed by the reactor, the support used to disperse the metallic phase is a key element in preventing carbon deposition. In a conventional reactor, the Ni/Al_2O_3 catalyst shows a good behaviour: low carbon deposition corresponding to the formation of reactive species that can be completely removed by hydrogenation. However, by the forcing of H_2 extraction, high amounts of low-reactivity deposits are obtained. A similar tendency is observed in the Ni/ZrO_2 sample under membrane reactor conditions, although this catalyst shows a higher disposition for generating this low-reactivity coke in a traditional reactor than does Ni/Al_2O_3.

The use of ceria-modified zirconia carriers changes the catalytic behaviour dramatically, depending on the structure and properties of the oxide support. Whereas Ni/ZrO_2–CeO_2 favours the formation of large amounts of coke in both membrane and traditional reactors (about 60 wt%), small amounts of reactive carbon species (about 4 wt% in the sample), which can easily be removed by hydrogenation, are formed on the $Ni/Ce_{0.5}Zr_{0.5}O_2$ catalyst.

The temperature-programmed hydrogenation (TPH) profiles obtained from the different samples used in the traditional and membrane reactors provide more information about the type of carbon species formed on each catalyst (Fig. 5). In general, the main hydrogenation product was CH_4, although in some cases some light hydrocarbons (C_2–C_3) and CO were also detected. As regards their reactivity with hydrogen, two types of hydrogenatable carbonaceous species have been found. The higher reactivity species, which can be hydrogenated at temperatures below 623 K and evolve as CH_4 (or light hydrocarbons in the case of the alumina-supported sample), have been assigned in the literature to the so-called C^{β} carbon. These species are probably formed from an amorphous structure in which carbon–carbon, carbon–metal, and hydrogen–carbon bonds are present. This type of carbon may include several subspecies, which differ in their mobility [27]. At temperatures above 673 K, low-reactivity graphitic carbon (C^{γ}) reacts

with hydrogen to yield CH_4, although it can also produce CO, depending on the support characteristics.

The TPH profiles obtained for the catalysts used under the traditional reactor conditions reveal important differences among the studied nickel samples, depending on the oxide carrier properties. In Ni/Al_2O_3 C^β and C^γ species are formed, showing the particularity of producing small amounts of light hydrocarbons at low temperature. Ni/ZrO_2 and Ni/ZrO_2–CeO_2 form mainly C^γ carbon, which at high temperature (above 773 K) evolves as CO and continues its production at temperatures above 1073 K. The presence of CeO_2 in the support stabilises some C^β species in the Ni/ZrO_2–CeO_2 catalyst, in contrast with the unpromoted sample. The production of certain amounts of CO during hydrogenation at high temperature is caused by the reduction of the support to a certain degree. The reducibility of ZrO_2, CeO_2, and Zr–Ce mixed oxides is related to the abundance of mobile oxygen in their structure and their capability to release it [28,29]. A completely different behaviour is obtained for the $Ni/Ce_{0.5}Zr_{0.5}O_2$ catalyst, for which only high-reactivity carbon (C^β) is obtained, in agreement with the gravimetric analysis.

The distribution of the hydrogenated carbon species is different for the samples used under the membrane reactor conditions. As a general trend, a transformation of C^β in C^γ is observed. C^β carbon only appears for the $Ni/Ce_{0.5}Zr_{0.5}O_2$ catalyst, in which some CO is also observed at high temperature as result of the reaction of C^γ carbon with oxygen released from the support. For the rest of the catalysts, C^γ species are observed to increase considerably in some cases, to the detriment of the more reactive C^β carbon.

The high tendency towards carbon deposition in the Ni/ZrO_2–CeO_2 sample under the traditional reactor operation conditions contrasts with the Ni/ZrO_2 behaviour. In general, CeO_2 addition to reforming catalysts as a promoter causes conversion to increase, although ceria-supported metals usually show very low activities for this reaction [29–31]. The utilisation of supports able to provide an extra source of oxygen (by favouring CO_2 activation through carbonate-, bicarbonate-, and/or formate-type intermediates or storing/releasing oxygen through a redox process) opens alternative pathways for the reaction, enabling a bifunctional mechanism [32–36]. However, in the case of CeO_2-supported catalysts and metals dispersed on CeO_2-impregnated supports, a typical behaviour has been observed: after an initial period of higher activity, a strong decay of the initial activity in the DMR reaction is usually found [17,30,37]. The redox properties of ceria and the high mobility of lattice oxygen are probably the factors that initially promote catalytic activity in the DMR reaction, but its easier reducibility under the reaction conditions probably causes a loss of the oxygen storage capacity of the support to provide active oxygen species.

The design of supports with high oxygen mobility that are chemically stable under reaction conditions has been proposed as the key to obtaining highly efficient and stable catalytic systems for the dry reforming of methane [17,31]. This is the case for mixed oxide Ce/Zr supports. Oxygen exchange experiments between the oxides and $^{18}O_2$ in the gas phase reveal the higher oxygen mobility in the Ce/Zr 1:1 mixed oxide in comparison with the pure oxides, ZrO_2 and CeO_2, and a CeO_2-impregnated ZrO_2 support, as shown in Fig. 6. Studies by computer-simulation techniques using atomistic models on surfaces of cubic CeO_2–ZrO_2 solid solutions have suggested that the increase in the oxygen storage capacity experimentally observed in these systems relative to pure ceria can be explained by the introduction of zirconia into the ceria lattice, a fact that decreases the Ce^{4+}/Ce^{3+} reduction energy on stable surfaces and increases the oxygen vacancies' tendency to segregate to these surfaces [38].

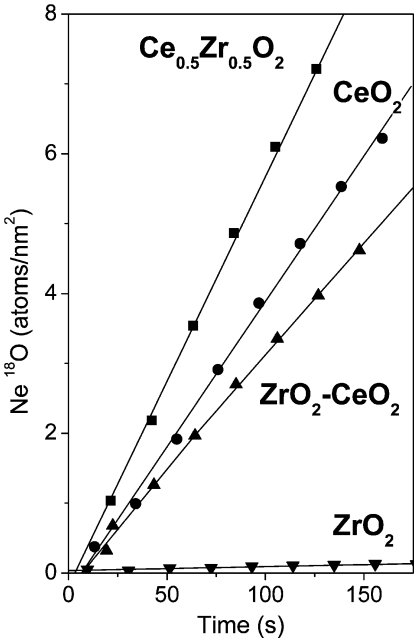

Fig. 6. Oxygen exchange rate of the oxides. Isotopic exchange carried out at 923 K with $^{18}O_2$ in the gas phase. (■) $Ce_{0.5}Zr_{0.5}O_2$, (●) CeO_2, (▲) ZrO_2–CeO_2, (▼) ZrO_2.

Therefore, the striking differences observed among the ZrO_2 and the two Ce-modified ZrO_2 nickel catalysts regarding to their resistance to carbon deposition can be attributed to the support characteristics associated with their different structures, as revealed by the XRD patterns of the samples (Fig. 7). The diffractogram corresponding to the Ni/ZrO_2–CeO_2 catalyst shows mainly the peaks corresponding to cubic ZrO_2, although signals corresponding to the monoclinic ZrO_2 phase can be also appreciated. No diffraction peaks corresponding to CeO_2 are observed, indicating that the promoter oxide is well dispersed on the ZrO_2 surface. The diffraction pattern of Ni/ZrO_2 indicates a different structure corresponding to tetragonal zirconia. Although cubic and tetragonal structures in ZrO_2 are difficult to differentiate, the broadening of the diffraction peaks at 2θ values close to 50.5° and 60°, probably due to diffraction line splitting, suggests the formation of the tetragonal phase [39].

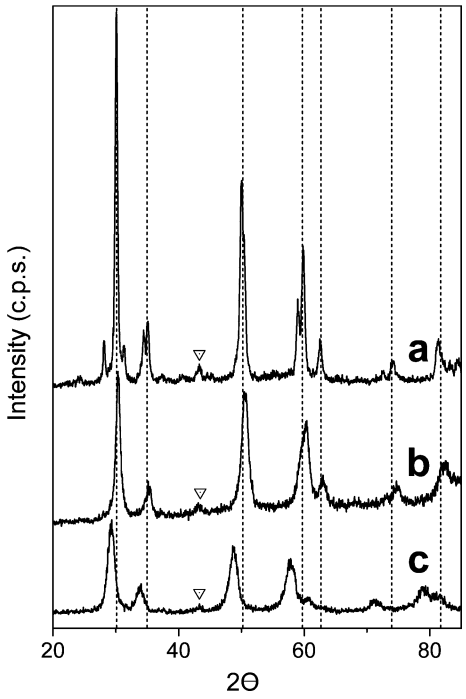

Fig. 7. XRD diffraction patterns of the fresh catalysts: (a) $Ni/ZrO_2–CeO_2$; (b) Ni/ZrO_2; (c) $Ni/Ce_{0.5}Zr_{0.5}O_2$. Dotted lines, diffraction lines corresponding to the cubic ZrO_2 phase. (▽) main diffraction peak of the NiO.

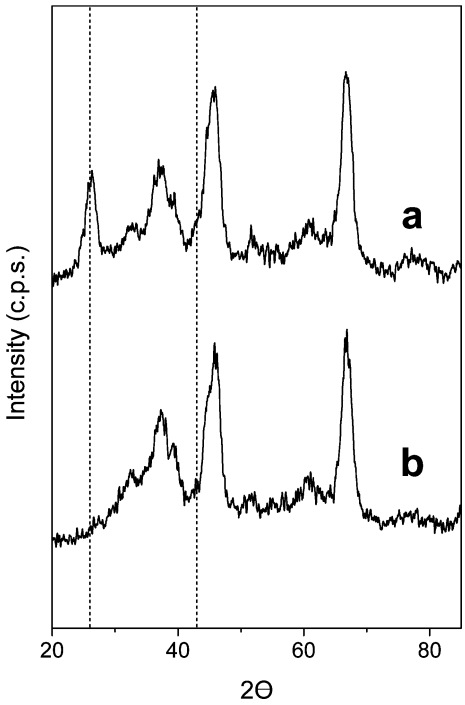

Fig. 8. XRD patterns of Ni/Al_2O_3 samples after 24 h operation in the reforming reaction ($CO_2/CH_4 = 1.9$): (a) membrane reactor; (b) traditional reactor. Dotted lines, diffraction lines corresponding to carbon fibres.

On the other hand, the mixed-oxide support prepared by the water-to-oil microemulsion method shows only the signals corresponding to the tetragonal $Ce_{0.5}Zr_{0.5}O_2$ phase diffraction [40]. Nagai et al. have recently studied the local structure of $CeO_2–ZrO_2$ mixed oxides with the same composition ratio. They have observed that the local arrangement in the oxide at the atomic level is the main factor determining the oxygen storage capacity (OSC) of this kind of material [41]: separated ZrO_2 and CeO_2 phases, or solid solution forms with Ce- and Zr-rich domains, show a much lower OSC than solid solutions of the same average composition homogeneously arranged.

Used catalysts were also examined by XRD after 24 h of operation in both membrane and traditional reactors. Figs. 8, 9, and 10 show the diffraction patterns obtained for the Ni/Al_2O_3, Ni/ZrO_2, and $Ni/ZrO_2–CeO_2$ samples. In agreement with the gravimetric weight variation analysis compiled in Table 2, the appearance of diffraction peaks at 2θ values of 26° and 46° is observed, corresponding to carbon nanofibres in samples showing high weight increases after reaction [42,43]. In the case of the $Ni/ZrO_2–CeO_2$ sample, signals corresponding to these carbon fibres are present in both samples used in the membrane reactor and in the conventional one. However, it can be appreciated that the reaction conditions affect the support structure, given that under the traditional reactor operation conditions the monoclinic ZrO_2 phase undergoes transformation into the tetragonal one. The Ni/Al_2O_3 and Ni/ZrO_2 catalysts give place to fibre formation only in the case of membrane reactor operation. However, in the latter, the incipient formation of these

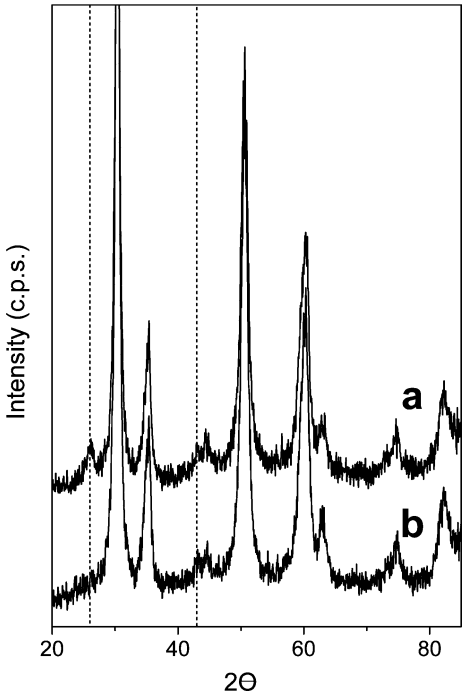

Fig. 9. XRD patterns of Ni/ZrO_2 (3.5% SiO_2) samples after 24 h operation in the reforming reaction ($CO_2/CH_4 = 1.9$): (a) membrane reactor; (b) traditional reactor. Dotted lines, diffraction lines corresponding to carbon fibres.

structures for the traditional reactor can be guessed from the XRD results, in concordance with the weight increase observed in the sample after reaction. No changes in the XRD

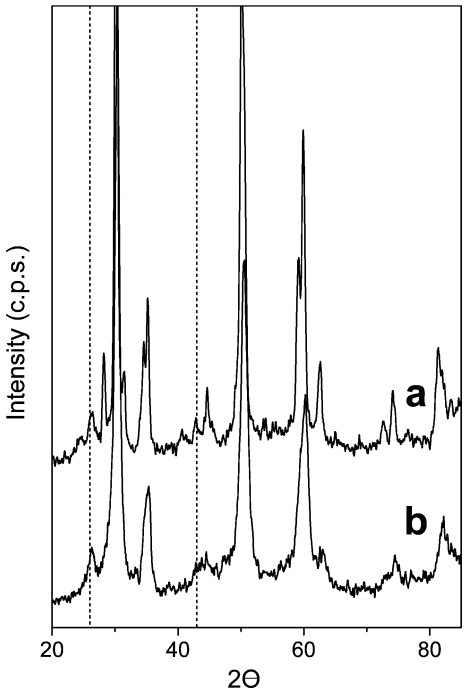

Fig. 10. XRD patterns of Ni/ZrO_2 (17.5% CeO_2) samples after 24 h operation in the reforming reaction ($CO_2/CH_4 = 1.9$): (a) membrane reactor; (b) traditional reactor. Dotted lines, diffraction lines corresponding to carbon fibres.

pattern were obtained for the $Ni/Ce_{0.5}Zr_{0.5}O_2$ catalyst, regardless of the reaction conditions.

These results regarding the presence of carbon fibres were confirmed by analysis of the samples by scanning electron microscopy (SEM). SEM photographs gave direct evidence of the kind of filamentous carbon structures formed on the different catalysts. Fig. 11 shows micrographs obtained from two distinct zones of the Ni/Al_2O_3 catalytic bed used in the membrane reactor. Although some catalyst particles remain free of filamentous carbon deposits, there are others that appear to be completely covered by very long carbon nanofibres with widths lower than 100 nm. The heterogeneity in the carbon deposition distribution is due to the presence of particles coming from different portions of the catalytic bed. Whereas conditions at the initial part of the fixed bed inside the membrane resemble those existing in a conventional reactor, catalyst particles located at the end of the catalytic bed operate under more unfavourable conditions due to the lack of H_2 and the high CO concentration.

On the Ni/ZrO_2 and Ni/ZrO_2–CeO_2 samples carbon deposits were more homogeneously distributed, probably because in these catalysts carbon deposition is more favourable, even when no H_2 is extracted from the reaction medium. Figs. 12 and 13 show micrographs obtained from these samples after 24 h of operation in the membrane reactor, in which carbon filaments are covering the catalyst surface.

A completely different aspect was found in the case of the $Ni/Ce_{0.5}Zr_{0.5}O_2$ catalyst, for which a carbon-free surface was found in most of the sample (Fig. 14a). However, the presence of small amounts of segregated ZrO_2, detected by energy dispersive spectroscopy, that do not form part of the mixed oxide, should be noted. These small particles, over which some carbon fibres have been found, are probably a very small portion of the whole catalyst, as they have not been detected in the XRD pattern, and the weight incre-

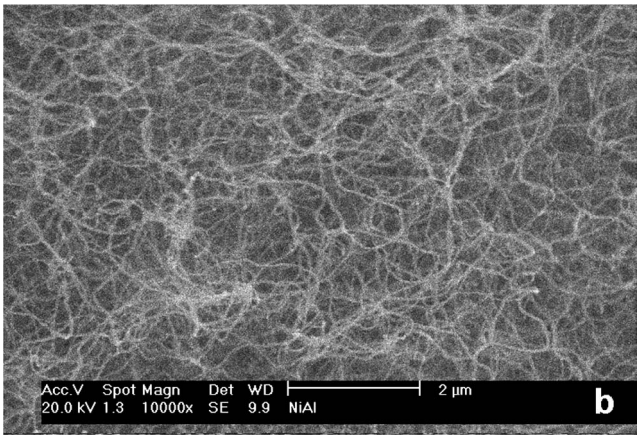

Fig. 11. SEM images obtained for the Ni/Al_2O_3 catalyst after 24 h operation in the membrane reactor. (a) and (b) are photographs of two different portions of the same catalytic bed.

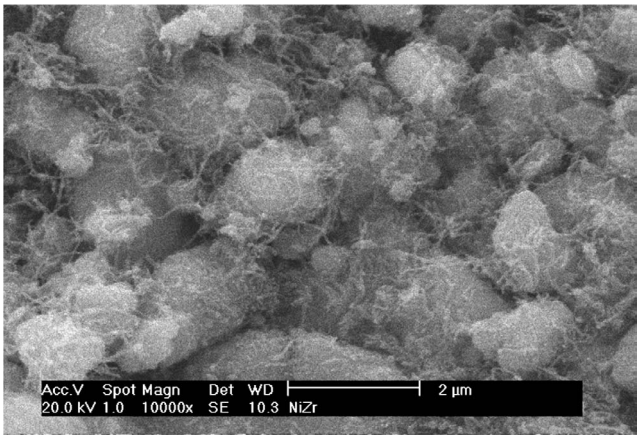

Fig. 12. SEM image obtained for the Ni/ZrO_2 catalyst after 24 h operation in the membrane reactor.

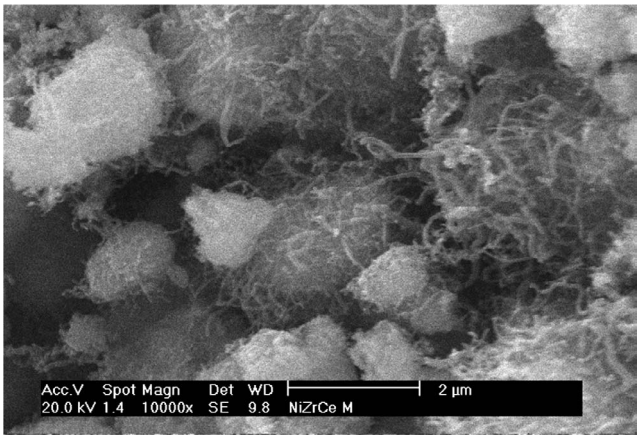

Fig. 13. SEM image obtained for the $Ni/ZrO_2–CeO_2$ catalyst after 24 h operation in the membrane reactor.

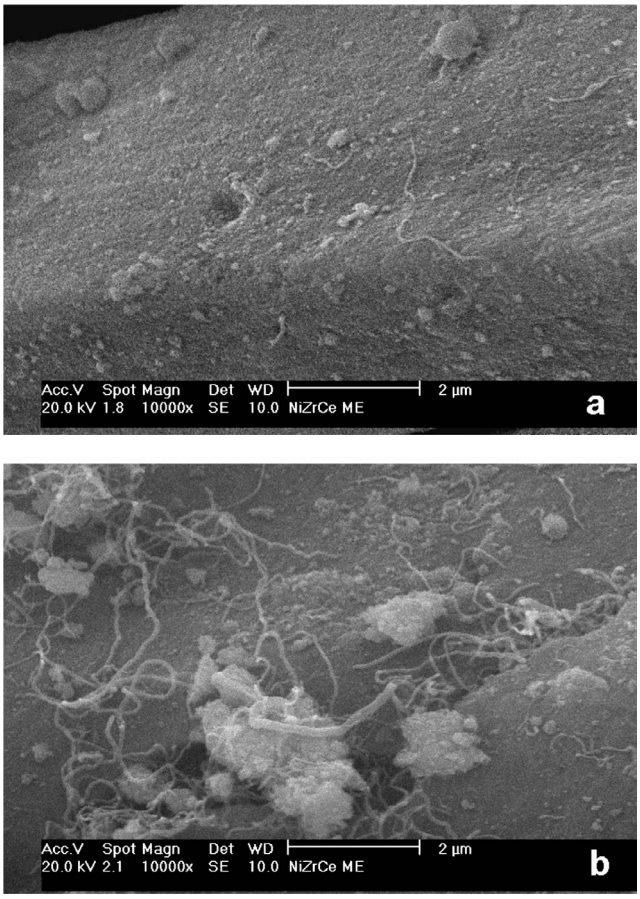

Fig. 14. SEM images obtained for the $Ni/Ce_{0.5}Zr_{0.5}O_2$ catalyst after 24 h operation in the membrane reactor: (a) surface of a typical catalyst particle; (b) detail of a particle covered with a segregated ZrO_2 phase in which some carbon nanofibres have grown.

ment corresponding to these carbon structures is negligible (Fig. 14b). Surface segregation of ZrO_2 in these mixed oxides has been described previously by Hori et al. [44].

Although carbon fibres are low-reactivity species with regard to H_2, they can be gasified and removed by reaction with CO_2, as found by Takenaka et al. over different nickel supported catalysts [43]. Their presence in distinct amounts on the several studied catalysts gives an indication of the relative rates between carbon deposition and removal. Transient kinetic studies on nickel catalysts have revealed that CH_4 adsorption and decomposition on Ni is a fast and reversible reaction step [45]. CO_2 dissociation is also fast, but the recombination of adsorbed carbon and oxygen species has been proposed as the process limiting the reaction rate. Despite the CO_2 excess used in the feed, the carbon deposition rate in some of the catalysts under the membrane reactor conditions is faster that its removal by reaction with CO_2, depending on the nickel support. This situation finally leads to the accumulation of huge amounts of carbon in the form of fibres. On the other hand, mixed-oxide-supported nickel ($Ni/Ce_{0.5}Zr_{0.5}O_2$) has exhibited excellent behaviour in reaction, even under the most severe conditions. Its capability to keep its surface free from carbon fibres seems to be due to its ability to release continuously extra oxygen from its lattice, to give it up to the nickel surface, thus enhancing the oxidation rate of the adsorbed carbon species.

One of the key issues for a membrane reformer is obtaining a long-lived, stable, high-performance catalyst that is resistant to carbon deposition. However, even when no carbon deposition is expected in the catalyst, it is desirable to use fluidised beds to obtain a homogeneous catalytic bed. Recently, interest in reactors that combine hydrogen-permeable membranes with fluidised beds for methane reforming has been growing [46–49]. This kind of system combines several advantages of fluidised beds as chemical reactors, particularly catalyst bed temperature uniformity and improved heat transfer, with advantages offered by permselective membrane technology: shifting the conventional thermodynamic equilibrium and obtaining a reaction product in a very pure state. In light of the presented results for a fixed-bed membrane reactor, for which carbon deposition in the reforming catalyst is associated with the different reaction atmosphere existing along the reactor length, fluidised-bed membrane reactors appear as a good alternative for solving these questions. The danger of abrasion, which is in fact a problem for unsupported palladium membranes in bubbling beds, is eliminated in the case of supported palladium films if they are synthesised on the surface opposite the reaction side. This would be one more step in reactor engineering design to use with stable catalytic systems to obtain a long-lived, high-performance reformer.

4. Conclusions

A palladium membrane reactor has been designed and sized for its application to the dry reforming of methane for pure hydrogen production. Several operation parameters (sweep gas flow rate, CO_2/CH_4 ratio, and CH_4 feed flow rate) have been adjusted to optimise the system performance with regard to CH_4 conversion, hydrogen recovery yield, and reduced carbon deposition. Four supported nickel

catalysts have been tested under the established conditions: Ni/Al_2O_3, Ni/ZrO_2, Ni/ZrO_2–CeO_2, and $Ni/Ce_{0.5}Zr_{0.5}O_2$. A detailed analysis of their behaviour under the severe conditions imposed by the reactor indicates that the oxide support clearly determines the catalyst resistance to carbon deposition. Among the tested catalysts, $Ni/Ce_{0.5}Zr_{0.5}O_2$ is the only one able to keep its surface free from carbon fibres, because of the high oxygen mobility in the mixed oxide and its chemical stability under reaction conditions. This high oxygen mobility support provides an extra source of oxygen for the oxidation of adsorbed carbon species on the metal surface, equilibrating in this way the rates of carbon deposition and removal on nickel and avoiding fibre formation.

Acknowledgment

P.F.-A. acknowledges the Spanish Ministry of Science and Technology for a Ramón y Cajal contract (call 2002).

References

[1] D.G. Löffler, K. Taylor, D. Mason, J. Power Sources 117 (2003) 84.
[2] L. Paturzo, F. Gallucci, A. Basile, G. Vitulli, P. Pertici, Catal. Today 82 (1–4) (2003) 57.
[3] B.S. Liu, L.Z. Gao, C.T. Au, Appl. Catal. A: Gen. 235 (2002) 193.
[4] A.K. Prahbu, S.T. Oyama, J. Membr. Sci. 176 (2000) 233.
[5] S. Uemiya, N. Sato, H. Ando, T. Matsuda, E. Kikuchi, Appl. Catal. 67 (1) (1990) 223.
[6] T. Ioannides, X.E. Verykios, Catal. Lett. 36 (1996) 165.
[7] A. Basile, L. Paturzo, Catal. Today 67 (1–3) (2001) 55.
[8] J. Múnera, S. Irusta, L. Cornaglia, E. Lombardo, Appl. Catal. A: Gen. 245 (2003) 383.
[9] E. Kikuchi, Catal. Today 56 (2000) 97.
[10] Y.-M. Lin, S.-L. Liu, C.-H. Chiang, Y.T. Chu, Catal. Today 82 (1–4) (2003) 127.
[11] E. Kikuchi, Fuel & Energy Abstracts 38 (2) (1997) 106.
[12] S. Irusta, L.M. Cornaglia, E.A. Lombardo, J. Catal. 210 (2002) 263.
[13] J. Shu, B.P.A. Grandjean, S. Kaliaguine, Appl. Catal. A 119 (2) (1994) 305.
[14] J.S. Oklany, K. Hou, R. Hughes, Appl. Catal. A 170 (1998) 13.
[15] K. Hou, M. Fowles, R. Hughes, Chem. Eng. Sci. 54 (1999) 3783.
[16] P.P. Mardilovich, Y. She, Y.H. Ma, M.-H. Rei, AIChE J. 44 (2) (1998) 310.
[17] S. Menad, P. Ferreira-Aparicio, A. Guerrero-Ruiz, I. Rodríguez-Ramos, Catal. Lett. 89 (1–2) (2003) 63.
[18] D. Sutton, S.M. Parle, J.R.H. Ross, Fuel Process. Technol. 75 (2002) 45.
[19] A.M. Gadalla, B. Bower, Chem. Eng. Sci. 43 (1988) 3049.
[20] I. Barin, O. Knacke, Thermochemical Properties of Inorganic Substances, Springer, Berlin/New York, 1973.
[21] Y.-M. Lin, G.-L. Lee, M.-H. Rei, Catal. Today 44 (1998) 343.
[22] Y.-M. Lin, M.-H. Rei, Int. J. Hydrogen Energy 25 (2000) 211.
[23] S. Goto, T. Tagawa, S. Assabumrungrat, P. Praserthdam, Catal. Today 28 (2003) 223.
[24] A. Effendi, K. Hellgardt, Z.-G. Zhang, T. Yoshida, Catal. Commun. 4 (2003) 203.
[25] G.F. Froment, J. Mol. Catal. A: Chem. 163 (2000) 147.
[26] T. Wurzel, S. Malcus, L. Mleczko, Chem. Eng. Sci. 55 (2000) 3955.
[27] T. Koerts, M.J.A.G. Deelen, R.A. van Santen, J. Catal. 138 (1992) 101.
[28] H. Vidal, J. Kaspar, M. Pijolat, G. Colon, S. Bernal, A. Cordón, V. Perrichon, F. Fally, Appl. Catal. B: Environ. 30 (2001) 75.
[29] H.S. Roh, K.-W. Jun, W.-S. Dong, J.-S. Chang, S.-E. Park, Y.-I. Joe, J. Mol. Catal. A: Chem. 181 (2002) 137.
[30] J.A. Montoya, E. Romero-Pascual, C. Gimon, P. del Angel, A. Monzón, Catal. Today 62 (2000) 71.
[31] F.B. Noronha, E.C. Fendley, R.R. Soares, W.E. Alvarez, D.E. Resasco, Chem. Eng. J. 82 (2001) 21.
[32] J.H. Bitter, K. Seshan, J.A. Lercher, J. Catal. 171 (1997) 279.
[33] P. Ferreira-Aparicio, I. Rodríguez-Ramos, J.A. Anderson, A. Guerrero-Ruiz, Appl. Catal. A: Gen. 202 (2000) 183.
[34] Z. Zhang, X.E. Verykios, S.M. MacDonald, S. Affrossman, J. Phys. Chem. 100 (1996) 744.
[35] J.H. Bitter, K. Seshan, J.A. Lercher, J. Catal. 176 (1998) 93.
[36] M.C.J. Bradford, M.A. Vannice, Appl. Catal. A: Gen. 151 (1997) 223.
[37] S. Wang, G.Q. Lu, Appl. Catal. B: Environ. 19 (1998) 267.
[38] G. Balducci, J. Kaspar, P. Fornasiero, M. Graziani, M.S. Islam, J. Phys. Chem. B 102 (3) (1998) 557.
[39] U. Martin, H. Boysen, F. Frey, Acta Crystallogr. Sect. B: Struct. Sci. 49 (1993) 403.
[40] S. Meriani, G. Spinolo, Powder Diffr. 2 (1987) 255.
[41] Y. Nagai, T. Yamamoto, T. Tanaka, S. Yoshida, T. Nonaka, T. Okamoto, A. Suda, M. Sugiera, Catal. Today 74 (2002) 225.
[42] S. Wang, Energy Fuels 12 (1998) 248.
[43] S. Takenaka, E. Kato, Y. Tomikubo, K. Otsuka, J. Catal. 219 (2003) 176.
[44] C.E. Hori, H. Permana, K.Y. Simon Ng, A. Brenner, K. More, K.M. Rahmoeller, D. Belton, Appl. Catal. B: Environ. 18 (1998) 105.
[45] Y. Schuurman, V.C.H. Kroll, P. Ferreira-Aparicio, C. Mirodatos, Catal. Today 38 (1997) 129.
[46] A.M. Adris, C.J. Lim, J.R. Grace, Chem. Eng. Sci. 52 (1997) 1609.
[47] T. El Solh, K. Jarosch, H.I. de Lasa, Appl. Catal. A: Gen. 210 (2001) 315.
[48] K. Jarosch, H.I. De Lasa, Chem. Eng. Sci. 54 (1999) 1455.
[49] Z. Chen, Y. Yan, S.S.E.H. Elnashaie, Chem. Eng. Sci. 58 (2003) 4335.